PROCEEDINGS OF SCIENCE

The JEM–EUSO energy and $X_{\max}$ reconstruction performances

F. Fenu*
Università degli studi di Torino, INFN Torino, RIKEN – Japan
E-mail: francesco.fenu@gmail.com

M. Bertaina, C. Vigorito

Università degli studi di Torino, INFN Torino

K. Shinozaki, A. Guzman, T. Mernik, A. Santangelo

Eberhard Karls Universität Tübingen

for the JEM-EUSO Collaboration

JEM–EUSO is an international collaboration committed to the development of space–based observatories for the study of cosmic rays at ultra–high energies In this framework we are carrying out an extensive simulation study in order to evaluate the performances of the mission. In this contribution we focus on the energy and $X_{\max}$ reconstruction performances. We therefore simulated several samples of cosmic ray events and we produced the detector response following a detailed simulation of the optics and of the detector. After the trigger recognized an excess, we analyze the received data to extract the basic shower parameters like direction, energy and $X_{\max}$. In this work we briefly describe the algorithms to reconstruct the energy and $X_{\max}$. We then present a study to assess the energy reconstruction performances in a set of fixed conditions and on the whole field of view. We also present preliminary results on the $X_{\max}$ reconstruction in the center of the field of view.

The 34th International Cosmic Ray Conference,
30 July- 6 August, 2015
The Hague, The Netherlands

*Speaker.

© Copyright owned by the author(s) under the terms of the Creative Commons Attribution-NonCommercial-ShareAlike Licence.

PoS(ICRC2015)604

1. Introduction

The Extreme Universe Space Observatory (EUSO) on–board the Japanese Experimental Module (JEM) of the International Space Station aims at the detection of ultra high energy cosmic particles from space [1]. JEM–EUSO is expected to observe ultra high energy (UHE) cosmic rays above and around the GZK threshold (E$\geq 4 \cdot 10^{19}$ eV), significantly increasing the exposure with respect to the current generation of ground–based observatories. Details on the expected science of JEM–EUSO can be found in [2, 3]. As stated in these references the main objective of the JEM–EUSO mission consists in the study of the anisotropy of the extreme energy sky and in the identification of ultra high energy cosmic ray sources. Also the study of the trans–GZK region of the spectrum must be considered as a priority. The requirements to achieve such results are listed in [3] and include a $\pm$30% in energy resolution above $8 \cdot 10^{19}$ eV. JEM–EUSO has also several exploratory objectives like the separation of photons and neutrinos from hadrons. As stated in the above mentioned studies a resolution in $X_{\max}$ of $\pm$120 g/cm^2 at 10^{20} eV and 60 deg zenith angle is considered satisfactory for this purpose. On the other hand, the determination of the mass of the hadron primaries is not one of the JEM–EUSO objectives.

JEM–EUSO consists of a UV telescope sensitive in the 300–400 nm band, which records the fluorescence tracks generated by cosmic rays propagating in the atmosphere with a time resolution of 2.5 microseconds. The detector consists of an array of $\sim$ 5000 Multi Anode Photomultipliers (PMT) organized in 137 PhotoDetector Modules (PDM). Each PMT is then subdivided in 64 pixels of 3$\times$3 mm size, covering a field of view on ground of roughly 500 $\times$ 500 m. The detector therefore consists of more than $3 \cdot 10^5$ pixels, which cover a field of view of 500 km diameter. The instrument will observe the Earth's atmosphere at night from a height of about 400 km, with a field of view of about 60 degrees. The observed geometrical area will be of $\sim 1.4 \cdot 10^5$ km^2 and the surveyed atmospheric mass will amount to about $\sim 1.5 \cdot 10^{12}$ tons of air. For details of the instrument, we refer the reader to [4, 5, 6]. For each observed event, the arrival direction, energy, and $X_{\max}$ must be reconstructed to recover the full observational information. In this paper, we show the preliminary results on the energy and $X_{\max}$ resolution obtained by the collaboration.

2. The energy and $X_{\max}$ reconstruction algorithms

The detailed description of the algorithms to reconstruct the energy and $X_{\max}$ parameters is out of the scope of the present publication. We refer the reader to [7, 8]. In Fig. 1 we give a sketch of the energy reconstruction algorithm. After the retrieval of the signal identified by the pattern recognition we start the correction of the inefficiencies of the detector, of the absorption in atmosphere and give an estimate of the fluorescence yield. The reconstruction of the geometry is done following either of two methods: the slant–depth or the Cherenkov method. As final result we will obtain a shower profile which we will fit with some predefined shower function [1]. In this way we obtain the energy and $X_{\max}$ of the shower.

We show in Fig. 2 an example of the reconstructed profile with the related fit. This event has an energy of $3 \cdot 10^{20}$ eV and has been reconstructed as $3.2 \cdot 10^{20}$ eV. The peak at the end of the profile is from Cherenkov light reflected on ground.

[1] In this case we use the so called GIL function or Gaisser Ilina Linsley. See [7] and [8] for more explanations.

PoS(ICRC2015)604

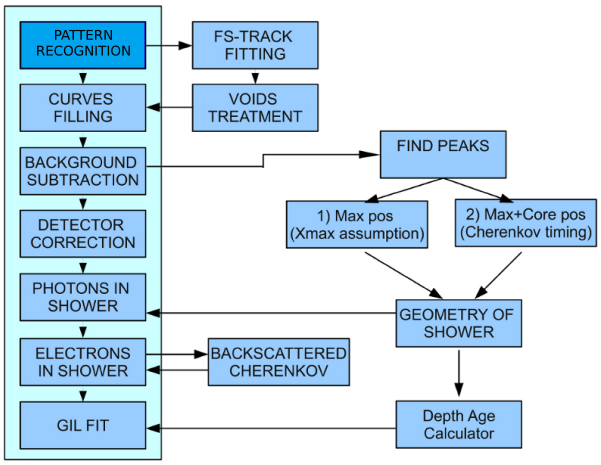

Figure 1: a simplified view of the energy and $X_{\max}$ reconstruction. The input information is represented by the blue box marker with the title *PatternRecognition*. Here the raw data is pre–processed and basic quantities such as the number of counts as a function of time are determined. Following the vertical path underlined in cyan, the counts curve is transformed according to a series of correction factors which are applied in each step. Complementary operations are executed on the right side of the diagram.

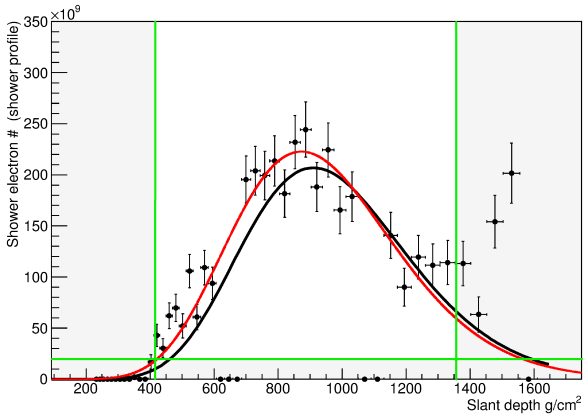

Figure 2: the simulated (black line) and reconstructed (points) shower electron curve. As a red line, the GIL fit (see text) can be observed. The simulated event has an energy of $3 \cdot 10^{20}$ eV and a zenith angle of 50 degrees. The reconstructed parameters for this fit are $3.2 \cdot 10^{20}$ eV and 873 g/cm^2 (whereas the real $X_{\max}$ was 915 g/cm^2). The χ^2 per degree of freedom is 0.905. The shaded areas show the points which are excluded from the fit.

3. Energy resolution

Using the reconstruction procedure discussed in the previous section, a study on the energy resolution of the JEM–EUSO mission has been performed for different zenith angles and different energies. The impact point is selected in the central part of the field of view (namely in the inner ($\pm$20,$\pm$20) km). Showers are generated according to the GIL parameterization. We simulated 8000 events for each point and we applied quality cuts DOF$>$ 4, $\chi^2/\mathrm{Ndf} < 3$ on all the conditions. To

PoS(ICRC2015)604

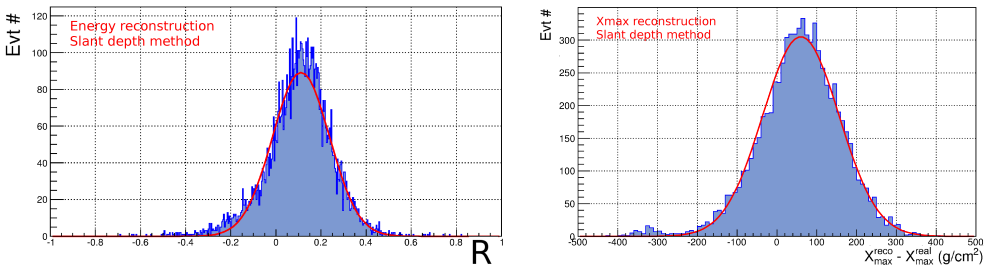

Figure 3: example of the resolutions obtained for showers with E = 10^{20} eV and incident angle of 45 degrees. The solid line denotes a Gaussian fit to the distributions. All the plots are referring to the central part of the field of view (namely in the inner (±20,±20) km).

estimate the resolution, we defined R as follows:.

$$R = \frac{E_{\text{reco}} - E_{\text{real}}}{E_{\text{real}}} \tag{3.1}$$

The distribution of the R for all the events which survived the cuts has then been fitted with a Gaussian curve. An example of the R distribution arising from the condition 10^{20} eV, 45 degrees has been shown in Fig. 3. As can be seen from the average of the distribution, the preliminary reconstruction algorithm presented here is biased and improvements are under study (see [7] for details). We also show here the Gaussian fit on this distribution. In the same plot we also show the corresponding distribution for the $X_{\max}$. In this case however we just consider for each event the difference between the reconstructed and real $X_{\max}$. The σ parameter of such a Gaussian fit is reported in Figs. 4, 5 and 6.

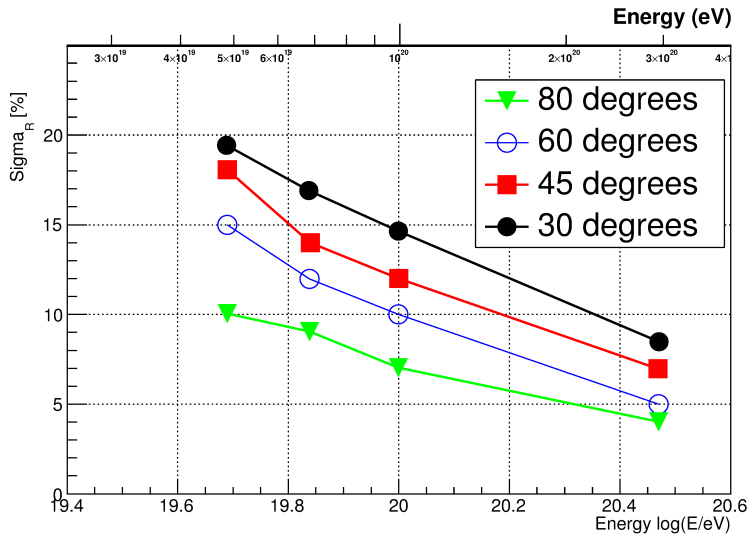

Figure 4: the Gaussian width of the R–distribution. Here, we plot the results for various zenith angles and energies. All the events are impacting in the central part of the field of view (namely in the inner (±20,±20) km). The geometry has been reconstructed with the slant–depth method.

As can be seen in Fig. 4, the energy resolution tends to improve toward the higher zenith angles. The resolution also tends to improve with the increasing energy due to the higher number

PoS(ICRC2015)604

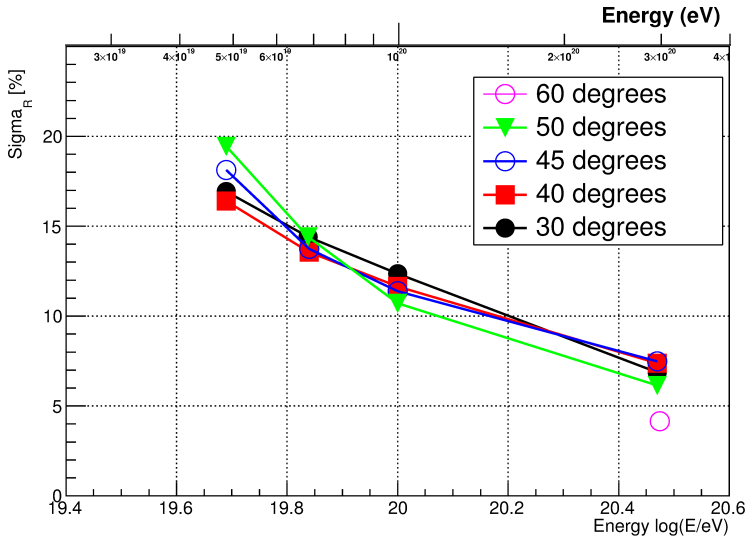

Figure 5: the Gaussian width of the R–distribution. Here, we plot the results for various zenith angles and energies. All the events are impacting in the central part of the field of view (the inner (±20,±20) km). The geometry has been reconstructed with the Cherenkov method.

of photons at the pupil. The slant-depth method has an energy resolution better than 20% At the most extreme energies, the resolution is better than 10%. In Fig. 5, the energy resolution obtained with the Cherenkov method is shown. Again, the highest energies allow the best performances, while a clear improvement depending on the zenith angle cannot be seen anymore. This is due to the worsening quality of the Cherenkov peak at the highest zenith angles. In fact, the Cherenkov peak will be much more difficult to recognize at the large zenith angles due to the larger spread of this reflection spot.

In Fig. 6, the energy resolution, estimated using the slant–depth method, is shown for events distributed in the range (±270,± 200) km and for energies in the range $2 \cdot 10^{19}$–$2 \cdot 10^{20}$ eV. The events have zenith angles between 0 and 90 degrees distributed as $\sin(2\theta)$. Here, we also apply DOF> 4, $\chi^2/\mathrm{Ndf} < 3$ quality cuts on $\sim 4 \cdot 10^4$ events. As can be seen, the resolution ranges from$\sim$ 30% at $2 \cdot 10^{19}$ eV to 15–20% at $\sim 10^{20}$ eV. The reconstruction bias has not been corrected and may still be contributing to the distribution width.

4. $X_{\max}$ resolution

A similar study has been performed for the $X_{\max}$ parameter. Using the samples described in the previous section (like in Figs. 4 and 5), we have calculated the distribution of the slant–depth of the maximum. In Figs. 7 and 8, we show the JEM–EUSO $X_{\max}$ resolution for fixed conditions of zenith angle and energy. Similarly as in the case for the energy, we evaluate the parameter $X_{\max}^{\mathrm{reco}} - X_{\max}^{\mathrm{real}}$ for all the events. We also fit the distribution with a Gaussian and we plot the σ parameter. An example of such distributions, with the corresponding Gaussian fit, can be seen in Fig. 3. In Fig. 7, we show the reconstruction performances for the slant–depth method. As can be seen the $X_{\max}$ resolution improves with the energy. At the lowest energies, it ranges from 90 to 120 g/cm^2 while

PoS(ICRC2015)604

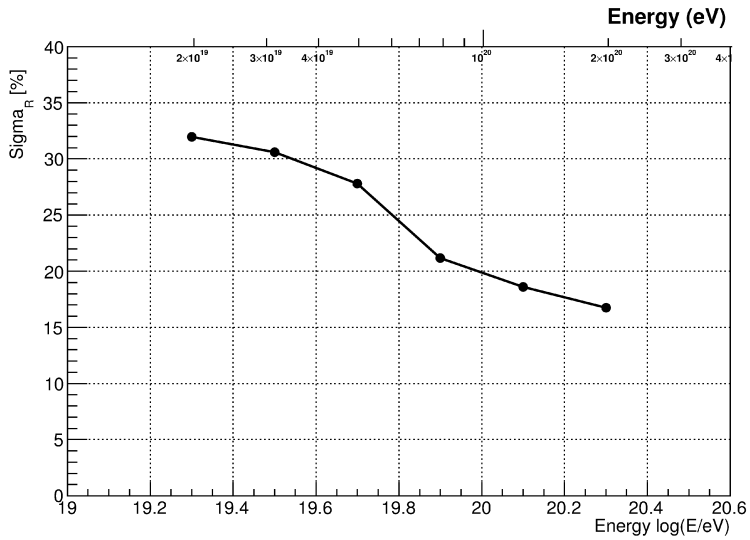

Figure 6: the energy reconstruction performances for the all–event sample. The points represent the σ_R value (multiplied by 100). The sample with cuts DOF> 4, $\chi^2/\mathrm{Ndf} < 3$ is shown here.

at the most extreme energies, from 60 to 80 g/cm^2. The resolution improves with zenith angle. This is due to the better angular resolution which can be achieved in these conditions. Moreover, showers incident at large zenith angles reach their maximum closer to the detector and therefore more photons are detected. The full longitudinal profile can be observed because it is not cut at ground level.

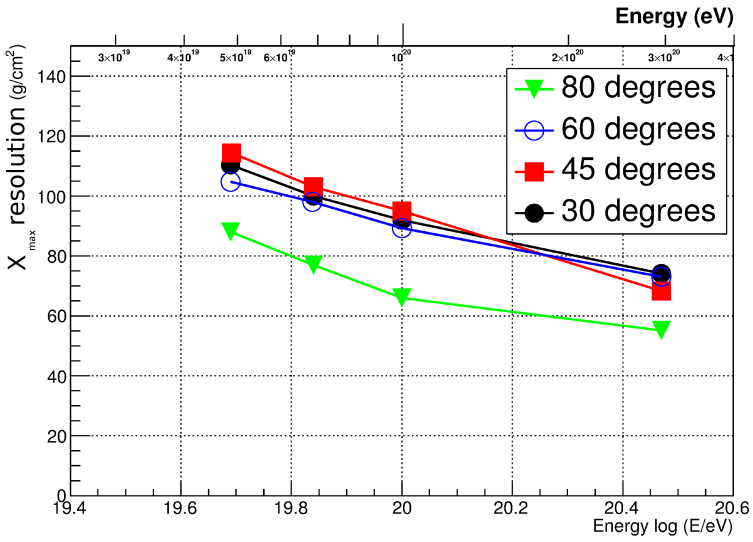

Figure 7: the Gaussian width of the $X_{\max}$ – distribution. Results are shown for different zenith angle intervals as indicated in the legend. All the events are impacting in the central part of the field of view (namely in the inner ($\pm$20,$\pm$20) km). The geometry has been reconstructed with the slant–depth method.

PoS(ICRC2015)604

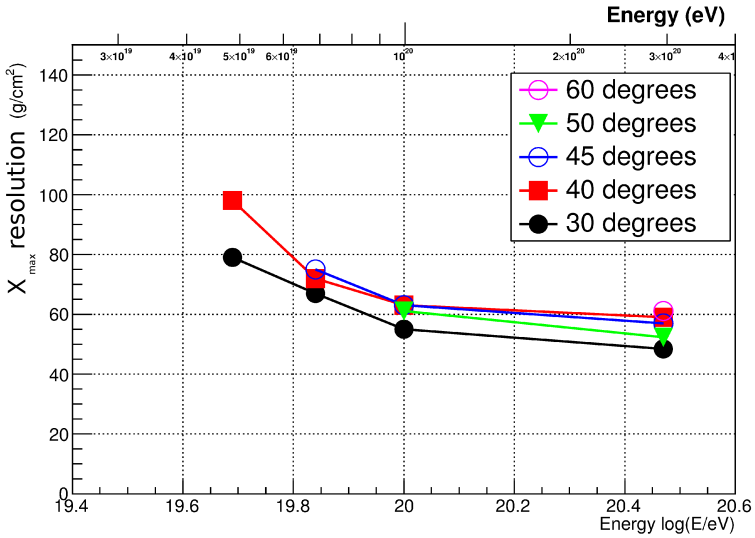

Figure 8: the Gaussian width of the $X_{\max}$ – distribution. Results are shown for different zenith angle intervals as indicated in the legend. All the events are impacting in the central part of the field of view (namely in the inner ($\pm$20,$\pm$20) km). The geometry has been reconstructed with the Cherenkov method.

In Fig. 8, the $X_{\max}$ reconstruction performances obtained with the Cherenkov method are shown. As can be seen here, the performances are significantly better ranging from 80–100 g/cm^2 at the lowest energies and 50–60 g/cm^2 at the highest. At the highest zenith angles the Cherenkov reflection peak will however not be recognizable. For this reason, the plots are only shown up to 60 degrees

5. Conclusions

To test the reconstruction algorithms, some preliminary example has been shown in fixed conditions, both for the energy and for $X_{\max}$. In fixed conditions, the energy resolution remains within $\pm$ 20% above $5 \cdot 10^{19}$ eV for both slant–depth and Cherenkov method. The resolution always improves with the energy reaching 5–10% at $3 \cdot 10^{20}$ eV for both methods.

In fixed conditions $X_{\max}$ is generally reconstructed within $\pm$120 g/cm^2 for the slant–depth method and within $\pm$100 g/cm^2 for the Cherenkov method. Here both algorithms also improve with the increasing energy reaching $\sim$ 50 g/cm^2 in both cases at $3 \cdot 10^{20}$ eV. The Cherenkov method will generally deliver a significantly better $X_{\max}$ resolution, especially for low zenith angles. The slant–depth method gives an $X_{\max}$ resolution which improves with the zenith angle, while the Cherenkov method shows a roughly zenith angle–independent performance.

The detection of a Cherenkov mark will allow a better energy and $X_{\max}$ reconstruction and will offer the possibility of a cross calibration of the two methods. A subclass of events will be reconstructed with the Cherenkov method which presents the best performances. In all of the cases where no Cherenkov peak will be detected, the slant–depth method will be used. The energy reconstruction performances have also been studied on the entire FOV and for zenith angles from 0 to 90 degrees but only with the slant–depth method. On the all–event sample (Fig. 6), the resolution

PoS(ICRC2015)604

is $\pm 15\%$ at $2 \cdot 10^{20}$ eV, while at the lowest energies it is $\pm 30\%$. We compare these results with the ones obtained in the center, which are always below 20%. The application of field of view cuts will, therefore, certainly improve the resolution.

As can be seen, the requirements on the energy resolution mentioned in the introductory part are clearly satisfied. Above $8 \cdot 10^{19}$ eV we can, in fact, achieve less than $\pm 25\%$ energy resolution against the $\pm 30\%$ requirement.

The $X_{\max}$ resolution within (± 20,± 20) km was found to meet the requirement of ± 120 g/cm^2. At larger distances, the resolution of the preliminary algorithm presented here is worse, but improvements are under study. It is worthwhile noting that even with the restricted central field of view, the exposure of JEM-EUSO will significantly improve the statistics currently available from ground-based detectors for exploratory studies of photon- and neutrino induced showers.

Acknowledgment: This work was partially funded by the Italian Ministry of Foreign Affairs, General Direction for the Cultural Promotion and Cooperation. We thank the original ESAF developers for their work. We wish to thank the RIKEN Integrated Cluster of Clusters facility for the computer resources used for the calculations.

References

[1] "The JEM–EUSO mission", T. Ebisuzaki et al., for the JEM–EUSO Collaboration, Advances in Space Research Vol. 53, Issue 10, 2014, Pages 1499–1505

[2] "Ultra High Energy Cosmic Rays studies with the JEM–EUSO mission" J. Adams et al for the JEM–EUSO collaboration, Experimental Astronomy Journal, this Issue's number 2 contribution.

[3] "Status of the JEM–EUSO mission", A. Santangelo for the JEM–EUSO collaboration, proceeding of the Int. Cosmic Ray Conference (Rio De Janeiro) (2013) – ID 0956

[4] "The JEM–EUSO instruments", F. Kajino for the JEM–EUSO collaboration, proceeding of the Int. Cosmic Ray Conference (Rio De Janeiro) (2013) – ID1216

[5] "An overview of the JEM–EUSO instrument", M. Casolino, F. Kajino, this Issue's number 8 contribution.

[6] "The Photodetector Module of the JEM–EUSO mission", S. Dagoret, P. Barrillon, A. Jung, A. Ebersoldt, this Issue's number 9 contribution.

[7] "Performances of JEM–EUSO: energy and $X_{\max}$ reconstruction", F. Fenu et al., Experimental Astronomy

[8] "A simulation study of the JEM–EUSO mission for the detection of ultra–high energy Cosmic Rays", F. Fenu, 2013, PhD Thesis, Tuübingen

PoS(ICRC2015)604